ORIGINAL PAPER

Study of FRP bars under tension using acoustic emission detection technique

Maha Ghaib[1] · Mohammadhadi Shateri[2] · Douglas Thomson[2] · Dagmar Svecova[1]

Abstract

Acoustic emission (AE) signal has proved to be a useful tool for monitoring structures reinforced with FRP composites such as Fiber Reinforced Polymer (FRP) reinforced beams, carbon FRP (CFRP) sheets, or steel fiber reinforced concrete. This work focuses on studying the behavior of pultruded FRP bars, which have been manufactured using continuous fibers. Different configurations of CFRP and glass FRP (GFRP) bar specimens subjected to tensile load were monitored using AE technique. Several algorithms were used for signal processing to analyze AE signals in the time domain and in the time–frequency domain. The signal processing techniques extracted the amplitude, cumulative events, duration, energy, rise time, number of counts, cumulative counts, and frequency peaks of the acoustic signals. The frequency maxima were determined for different amplitude signals using short-time Fourier transform (STFT). Cumulative counts of AE signals showed significant changes in the slope during the tension test, while the stress–strain relationship of the FRP rods showed virtually no deviation from linearity. CFRP bars recorded higher amplitude signals and lower duration, than GFRP bars. The acoustic emission characteristics presented in this work show strong correlations with ultimate load and may prove useful for damage prediction.

Keywords Acoustic emission · Carbon fiber reinforced polymer (CFRP) · Glass fiber reinforced polymer (GFRP) · Tensile load · Scanning electron microscopy (SEM)

1 Introduction

CFRP and GFRP bars have been used widely in concrete structures for the past quarter century, either to rehabilitate damaged reinforced and pre-stressed concrete elements, or to reinforce new ones [1–3]. As of 2016, 65 bridges have been built using FRP bars in the USA, and 202 bridges have been built using FRP bars in Canada including bridge decks, parapets, barriers, and sidewalks [4]. The advantages of using FRP are high strength to weight ratio, corrosion resistance, nonconductive properties, durability, and high tensile strength [4]. However, FRP bars have a brittle behavior and demonstrate a linear stress–strain curve up to failure. It would be beneficial to have non-destructive testing (NDT) methods that have the potential to detect damage at loads well below failure. This is particularly important for FRP bars as they do not exhibit any external signs of damage until brittle failure.

The AE technique has been used for decades, in several fields, as a structural monitoring technique [5]. It has been used to inspect structures such as pipes, vessels, storage tanks, concrete, rock, wood, superstructures of buildings and bridges, and substructures including railway structures and nuclear power plants [5]. AE signals are transient elastic waves generated by a sudden release of energy from localized sources within a material [6]. These waves could be due to damage such as cracking in reinforced concrete

✉ Maha Ghaib
   ghaibm@myumanitoba.ca

   Mohammadhadi Shateri
   shaterim@myumanitoba.ca

   Douglas Thomson
   Douglas.Thomson@umanitoba.ca

   Dagmar Svecova
   Dagmar.Svecova@umanitoba.ca

[1]   Department of Civil Engineering, University of Manitoba, Winnipeg, Canada

[2]   Department of Electrical and Computer Engineering, University of Manitoba, Winnipeg, Canada

structures [7], or degradation resulting from the corrosion of reinforcing steel bars in concrete structures [8]. In FRP materials, acoustic emission could be due to fiber breakage, matrix cracking (both micro and macro), delamination, debonding, fiber cracking, or fiber pullout [9].

An advantage of the AE technique is that it has the ability to monitor a region or volume of a structure in one test by attaching an array of AE sensors. This is possible because the method does not require a priori knowledge of the location of the defect. Therefore, it is an attractive method for monitoring materials in larger structures.

2 Literature review

Several studies have been conducted using AE signals to correlate their amplitude and frequency to damage occurrence in FRP composites such as laminates [10] and stay cables [11]. The range in frequencies and amplitudes varies depending on the type of signal. It was found that certain amplitudes and frequencies are predominant for matrix cracking, while others correspond to fiber pullout or fiber breakage [10, 12–14]. A study has been conducted to find the source location using aramid FRP plastics subjected to tension and monitored by AE technique [15]. The results showed that the failure occurred at different location through the sample length and that peak amplitude distribution was affected by the attenuation [15]. Damage location in hybrid FRP bars was determined using AE and fiber optic single-channel acoustic emission sensors [16]. Both AE and fiber optic single-channel acoustic emission sensors were equally successful in locating damage and both had maximum errors near the middle of the bar. The spectral energy method was effectively used to distinguish between the fracture of carbon and glass fibers [16]. Additional study has been conducted to assess damage mechanisms of a beam post tensioned by hybrid FRP tendons using AE technique [17]. The study showed the ability of AE to localize the damage at different stages of the loading and to determine the pseudo yield point of the post tensioned beam by determining the cumulative spectral energy for both carbon and glass fiber. They also validated the results with the load deflection response [17].

Research has been conducted to test different types of CFRP and GFRP bars under ramping load for pultruded FRP bars manufactured using continuous fibers and used in civil infrastructure. The histogram of the counts in every 10 s interval and the cumulative of these counts were plotted. The results showed that the count rate increases with increasing load, with a maximum peak count rate occurring near failure. Also, the results showed that GFRP generated AE events at an earlier stage than the CFRP [18].

Frequency analysis has been conducted in several studies for FRP composites, though no general basic ranges have been established to correlate specific frequency bands to specific damage mechanisms. The ranges are specific to materials and tests used. However, most of the results conclude that the highest frequencies correlate to fiber breakage and the lowest ones correlate to matrix cracking [19, 20]. Fast Fourier Transform (FFT) is generally used to recognize the signal frequency content, but it is unable to record information about the time of frequency occurrence. Since AE waveforms are presented in both time and frequency domains and provide valuable data, joint time–frequency technique is important. Wavelet Transform (WT) and STFT analyses are powerful time–frequency techniques that can provide pertinent information from AE signals to determine damage types in composites [21, 22]. Kaphle et al. [22] obtained similar patterns of the frequency bands for both WT and STFT methods. STFT calculates the Fourier transform by dividing the signal into stationary parts; a short window function is used to extract the parts from the original signal, and then the window is relocated to a new location for the next calculation. The result obtained from the new location of the window is the time–frequency localization, which has a constant localization resolution due to the limited length of the window. Information about the energy and frequency content at a specific time can be obtained using this method.

In this study, STFT was performed for calculating FFT and energy. Spectrograms using MATLAB were used to obtain the frequency bands that are predominant for both CFRP and GFRP bars at each load level during the test.

Kaphle et al. [23] calculated the energy distribution in the AE signals by using an STFT matrix. The coefficients of this matrix are $C(\omega_i, \tau_j)$, where ω_i represents FFT in rows and τ_j represents time in columns. The normalized energy ratio as a function of frequency $(E_{(\omega)})$ can be calculated as follows:

$$E_{(\omega)} = \frac{\sum_{J=1}^{N} C^2(\omega_i, \tau_j)}{\sum_{i=1}^{M} \sum_{j=1}^{N} C^2(\omega_i, \tau_j)}, \tag{1}$$

where N is the numbers of columns that represent the time, and M is the number of rows that represents the frequency. Studying energy distribution in the time–frequency domain is expected to provide important information about the nature of the damage source. Energy distribution does not vary with the change of the distance between the sensor and the source, i.e. it is not affected by the signal attenuation [23]. Energy distribution as a function of frequency was performed to find the frequency bands that are predominant in specific signals.

Scanning electron microscopy (SEM) identified damage mechanisms in continuous unidirectional GFRP

composites and has been correlated to AE signals by using different span to depth ratio samples subjected to testing in three-point bending [24]. Another study has been used SEM to observe damage mechanisms of different glass/polypropylene plate samples subjected to tensile loads [25]. Different fiber orientations were used in the study: 0°, ± 45°, 90°, (0°–90°) for each sample [25]. Previous studies have not addressed AE correlation with SEM on FRP bars. The work presented in this paper will use SEM to compare microstructure of FRP pultruded bars before testing and at failure to aid in identifying the origin of AE signals recorded during load tests.

3 Typical AE signals

AE is a wave generated by a sudden release of energy. The strength of acoustic signals is determined by the damage growth, the distance between the damage source and the sensors, and the acoustic properties of the transferring material [26]. After amplification and digitizing, an AE signal is represented as a voltage vs. time plot. It can be characterized using several parameters, as shown in Fig. 1. By applying these parameters, damage initiation and development can be monitored. The definition of these parameters can be found in [27].

AE waveforms can be classified using several of the AE parameters that can be related to different stages of the tensile test. Figure 2 shows AE signals for CFRP and GFRP that have different amplitudes. For the highest peak amplitude signals, some non-linearity can be observed. For peak amplitudes exceeding 80 dB_{AE} there is an offset in the

signal before and after the AE event that is an artifact of instrumentation. These results overestimate the peak amplitude at the largest signal levels (> 95 dB_{AE}) of up to ~ 1.6 dB. For peak amplitudes of less than 80 dB_{AE} this offset is not observed. The duration of the AE signals ranges from 27.5 microseconds to several milliseconds.

4 Experimental procedure

4.1 Specimen preparation

AE signals were generated from different GFRP and CFRP bar specimens subjected to ramping tensile loads. CFRP rebar specimens were manufactured using 27% of epoxy vinylester-based resin and 73% of carbon fibers; GFRP rebar specimens were manufactured using 27% of vinylester-based resin and 73% of fibrous glass. The bars chosen for this study are commonly used for reinforcing applications. The two bar diameters were chosen to see if bars of smaller and larger diameter have similar AE characteristics. CSA S806 (2012) Annex B was used to prepare the specimens [28]. The code requires that the tension force be applied to the samples indirectly to prevent FRP crushing in the anchorage zone. As a result, FRP specimens were anchored into steel pipes that were gripped by the testing machine. Servo-hydraulic load system was used for the tensile loading test as shown in Fig. 3. Strain gauges with gauge length of six millimeters and resistance of 120 $\Omega \pm 0.3\%$ were placed on the surface of each specimen at the center of the bar. A brief description of the FRP types and their configurations is shown in Table 1.

4.2 AE apparatus and software

Signal processing involves signal transference, amplification, filtering, and feature extraction [29]. In this study, a piezoelectric transducer (R15I-AST Physical Acoustic Corporation) was used for sensing the AE signals. The R15I-AST sensor 80–200 kHz contains an integral 40 dB preamplifier that amplifies the signal to reduce the effects of noise. The sensor was attached firmly to the surface of the anchors by plastic cable ties and a stainless-steel hose clamp. A layer of Proceq couplant gel was used between the sensor and the surface to eliminate air gaps and to ensure good transmission of AE signals from the surface to the sensor. Experimental set up of the AE monitoring system for the tensile load testing is shown in Fig. 3. The signal was digitized using an analog to digital converter (DT9816-S 16 bit with maximum 750 kHz sampling rate, Data Translation Inc.). The sampling rate was set to 400 k samples/s. The amplitude threshold for detection of acoustic events was set to 46 dB_{AE}. This level is
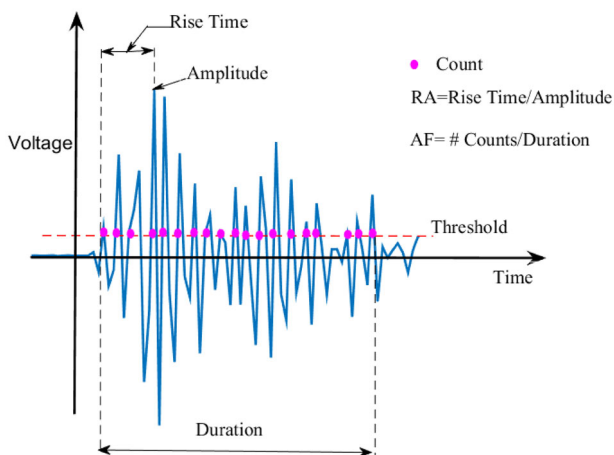

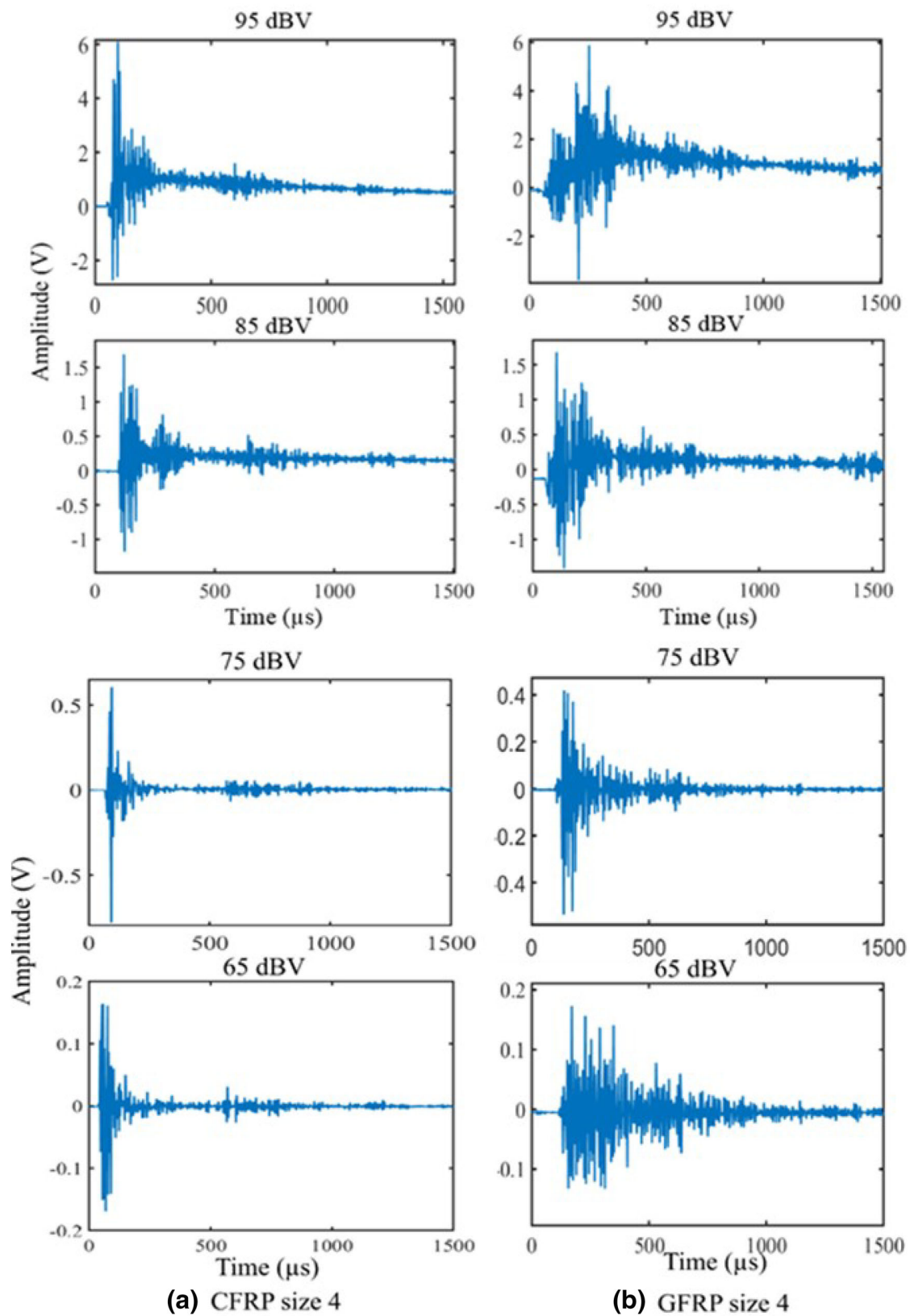Fig. 1 AE signal characteristics. Amplitude is the maximum voltage peak; duration is the time of a signal from the first point exceeding the threshold level to the last one; counts is the number of times which AE signal crosses the threshold level; Rise time is the time measured from the first point of the signal that exceeds the threshold level to the maximum peak amplitude [27]

Fig. 2 Typical unfiltered AE signal at 98, 85, 75, and 65 dB$_{AE}$ for **a** CFRP and **b** GFRP size 4 ($d = 13$ mm)

Fig. 3 AE system set up for the tensile load testing. **a** FRP specimen with anchors in servo-hydraulic load frame. **b** Sensor coupled to the anchor using couplant gel
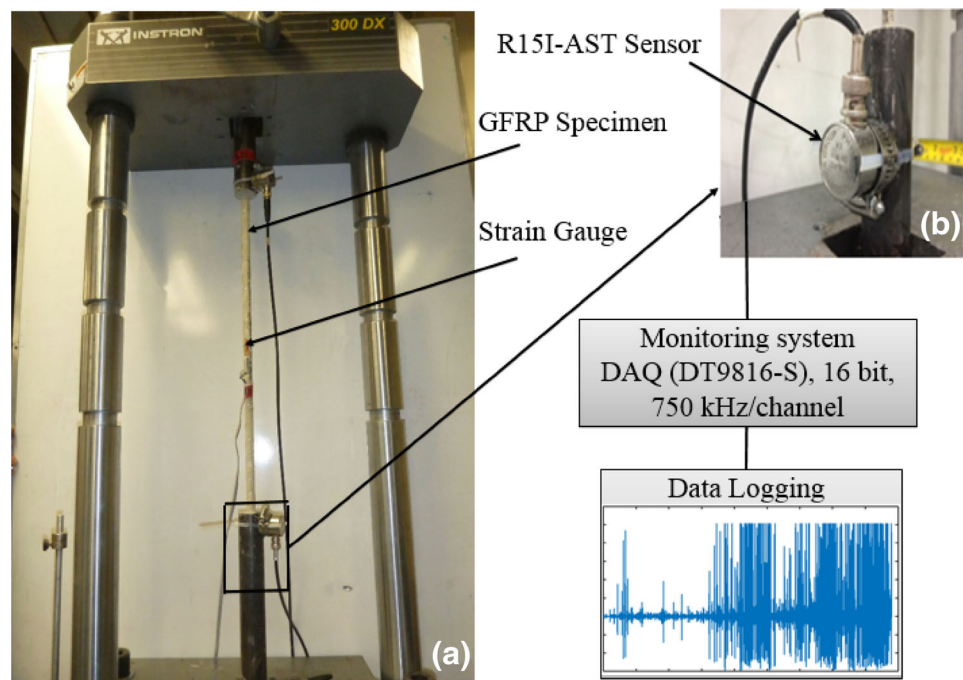

Table 1 Summary of FRP test specimens and their loading conditions

Bar type	Number of specimens	Diameter d (mm)	Tensile strength f_u (MPa)	Specimen length (40d) mm	Anchor length (f_u*A/350) ≥ 250 (mm)	Loading rate (kN/min)
CFRP size 2	5	6	2241	240	250	13[a]
CFRP size 4	5	13	2068	520	800	45
GFRP size 4	5	13	758	520	300	60*
GFRP size 6	5	19	690	760	600	80

[a]Tested under displacement control

approximately ten times the typical observed peak to peak noise amplitude and hence produces few false triggers. A pencil lead break (PLB) test was performed near the sensor before any AE data recording in order to check the sensitivity of the sensor and the functioning of the amplifier and DAQ.

AE was applied to investigate the fracture of different diameters of CFRP and GFRP bars during tensile loading. A burst AE signal was generated every time material components undergo cracking or fracture. The response of these signals was analyzed to identify their sources, using conventional signal analyses in time domain. Amplitude distribution over time, cumulative ratio of the amplitude distribution corresponding to the percentage of the ultimate load, RA (rise time divided by amplitude) and AF (number of counts divided by duration) as a function of time,

cumulative counts, and amplitude versus duration, were plotted for this purpose. AE parameters definitions were provided in the caption of Fig. 1.

5 Attenuation measurement

The attenuation of AE signals along the FRP rebars was determined experimentally. To achieve reproducible PLB tests, the pencil was held at the same angle and orientation to the FRP bar surface using a foam ring. The lead was also extended to the same length for each PLB. Fifteen locations were sampled on the FRP bar, once every 5 cm between sensor 1 to sensor 2. For each location, six pencil-lead break tests were done and the average amplitudes were used. The amplitude of the AE signals for sensor 1 and

sensor 2 can be modeled using the following equations [30]:

$$A_1 = A_s \times C_1 \times e^{-\alpha(L+x)} \tag{2}$$

$$A_2 = A_s \times C_2 \times e^{-\alpha(L-x)}, \tag{3}$$

where A is the amplitude at AE source and C_i is used due to differences in coupling between sensor and material surface or due to sensitivity of the sensor.

The ratio of peak amplitudes that was detected at both sensors for AE sources originating from different locations along the bar was used in order to estimate the attenuation α. Figure 4 shows an example of AE signals that were generated from the PLB test and the peak amplitudes that were used for the attenuation measurements for GFRP size 6 bar.

Using Eqs. 2 and 3, the slope of natural log of (A_1/A_2) versus distance can be used to find the attenuation. Linear regression was used and the slope of the line shown in Fig. 5 was found to be 0.43 dB/cm. The correlation constant r of the regression was calculated as 0.983 following the procedure in [31].

6 Results and discussion

6.1 AE signal analysis in time domain

The three-part RMS algorithm described in [32] was used to separate one event from another. For each AE event, a number of parameters were measured such as amplitude, duration, number of counts, rise time, peak frequency, and average frequency.
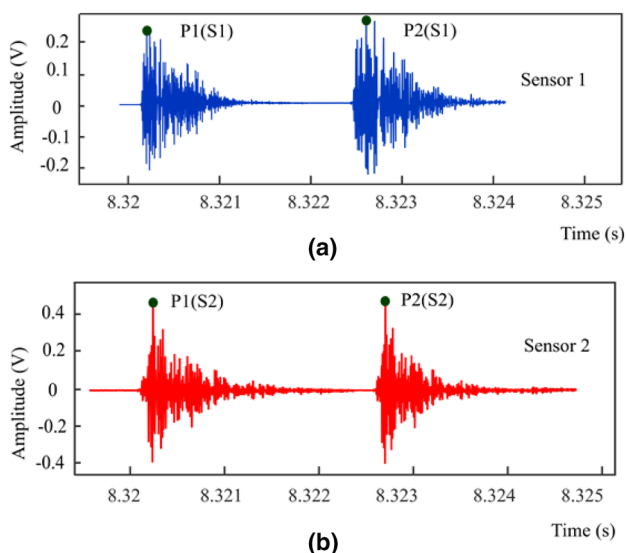

Fig. 4 Example of the PLB test result for both sensors at $x = 25$ cm. **a** PLB recorded by sensor #1; **b** PLB recorded by sensor # 2
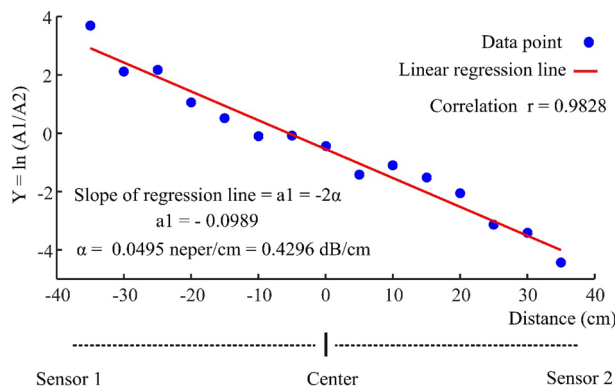

Fig. 5 Attenuation measurement using linear regression on the PLB test data

6.1.1 Amplitude

Twenty tests in total were carried out on different diameters of CFRP and GFRP reinforcing bars. Each of the tests had similar trends in the AE parameters. Therefore, only typical plots are presented.

Evolution of the peak amplitude of individual AE signals over time is shown in Fig. 6. In Fig. 6, each AE event is presented as a single dot on the plot. In total 146–811 events per cm^3 were observed in the GFRP size 4 bars, 157–792 events per cm^3 in GFRP size 6 bars, 557–4578 in the CFRP size 2 bars, and 48–604 in the CFRP size 4 bars. The voltage threshold for detection of acoustic events was set at 46 dB$_{AE}$, and hence there are no events below this threshold. Two interesting observations can be made from Fig. 6. First, the number of events per unit time increases as strain level increases. The direction of the loading is parallel to the fibers and in past work the low and medium amplitude levels have been attributed to debonding between the fibers and matrix and the longitudinal microcracks in the matrix [12, 33, 34]. Fiber breakage was thought to release more energy per event and has been attributed to the higher amplitude AE signals [35, 36]. Second, the number of higher amplitude signal events per unit time also increases with strain levels.

At early stages of the test, CFRP bar specimens had higher amplitude signals than the GFRP specimens. The mean ratio of the high-amplitude signals to the low- and medium-amplitude signals, for the five CFRP specimens, was 4 and 6% for size 2 and 4, respectively. In contrast, the GFRP specimens had a very small fraction of high-amplitude events relative to the low- and medium-amplitude events. The average ratio of the high-amplitude signals to the low- and medium-amplitude signals for five test specimens was 1% for both size 4 and 6 bars.
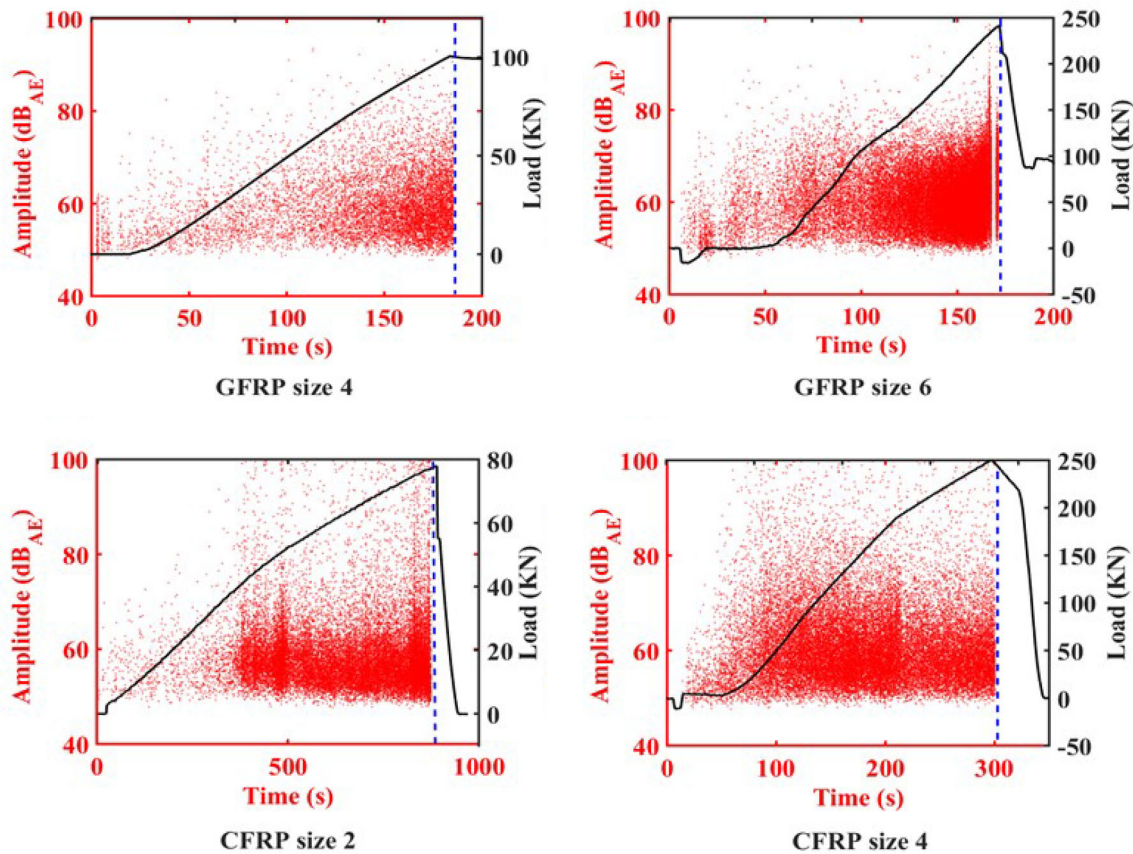
Fig. 6 Amplitude vs. time with load time superimposed. Dashed line represents time at which failure occurred for CFRP size 2 and GFRP size 6. CFRP size 4 and GFRP size 4 were loaded up to 93 and 95% predicted ultimate load, respectively

6.1.2 Average frequency (AF) and RA value and cumulative counts

Average frequency is calculated by dividing the number of counts by the duration, for one hit [5]. RA value is calculated by dividing the rise time, by the amplitude of the hit [5]. The rise time is the time interval from the start of a detected hit to the maximum amplitude of a hit. These parameters have proven useful in linking AE event characteristics to the types of physical damage and damage accumulation [37, 38]. These two parameters have been used to link AE events to the type of cracks in concrete materials and have been standardized in JCMS-III B5706 for active cracks in concrete [39].

In concrete materials, high RA value is an indication of shear cracks, while the low RA value refers to the tensile cracks [37, 38]. In transportation structures, high RA value and low AF have been attributed to traffic induced noise [40].

Soulioti et al. studied RA and AF parameters of AE signals from concrete containing different percentages of steel fiber under four-point bending [41]. They concluded that the damage mode changed from tensile to shear as

fiber content increased in concrete. This resulted in an increasing RA and decreasing AF [41]. In laminated composites, a similar change has been associated with a transition from matrix cracking to delamination [42, 43].

AF and RA values of AE signals during tensile loading were calculated and plotted as function of time for CFRP bars in Fig. 7 and for GFRP bars in Fig. 8. For each type of bar, five samples were loaded up to failure and the average of their ultimate loads was taken to be the predicted ultimate load. Cumulative counts were also plotted together with stress–strain curves. Thirteen CFRP and GFRP samples were loaded up to failure, while seven were loaded up to 64–95% of the predicted ultimate load. This saved the samples from being totally destroyed, so that they could be used later for SEM analysis. High RA value and low AF were observed at the start of the test, up to 10–20% of the predicted ultimate load as shown in Figs. 7a, b and 8a, b. AE signals of this type have been associated with friction between the machine grip and may also be due to the anchor [44]. After this early region, the AF and RA became relatively steady with some fluctuations. However, the magnitude of these early AE signals was variable in some tests, which had relatively lower initial levels of these
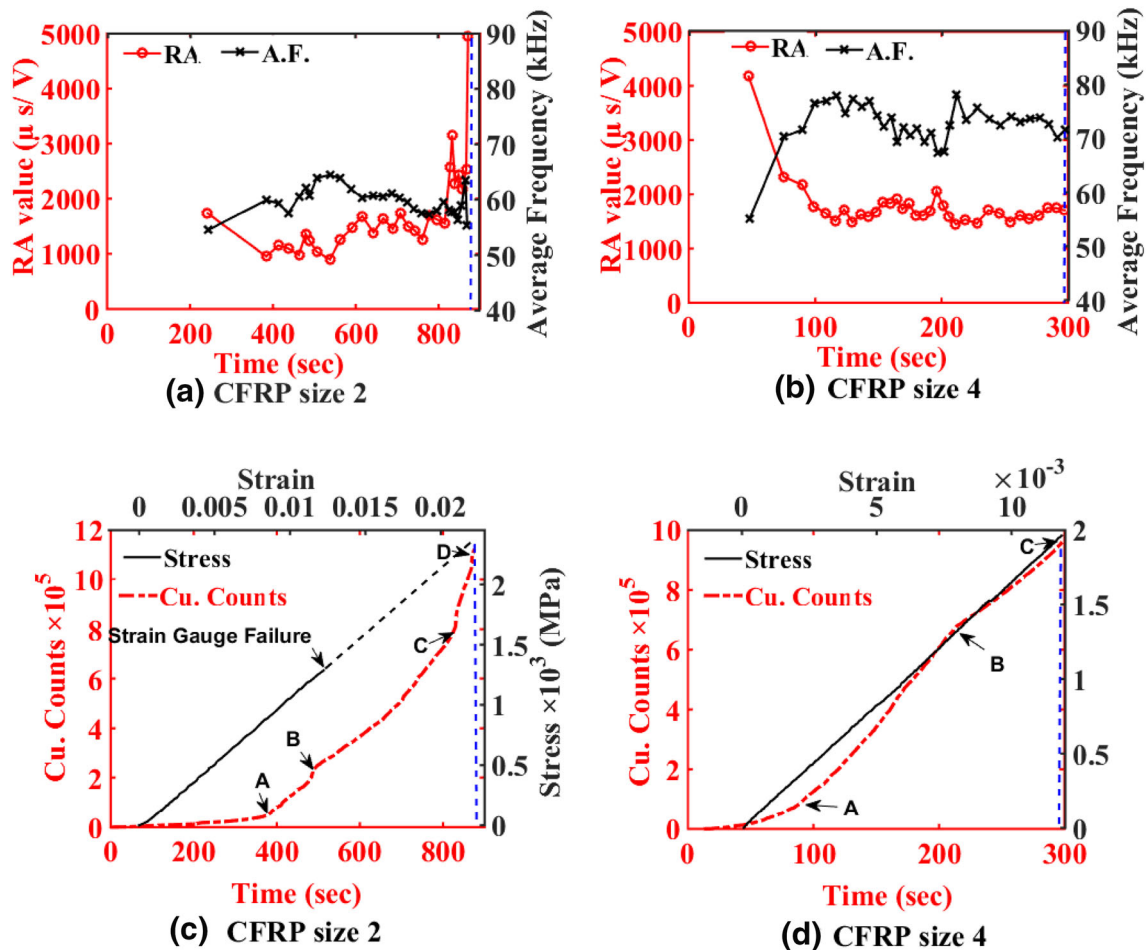
Fig. 7 Variation of AF and RA values. Cumulative counts vs. time with stress–strain superimposed. Dashed line represents time at which failure occurred for CFRP size 2. CFRP size 4 was loaded up to 93% of the predicted ultimate load. CFRP size 2 specimen was tested under displacement control (Table 1)

signals. As the load increases there is an increase in the slope of cumulative counts curve (point A) in Fig. 7c, d that is associated with an increasing rate of internal damage for CFRP bars.

In contrast, GFRP bars show a linear increase of the cumulative counts curve up to 40% of the predicted ultimate load (point A), as shown in Fig. 8c, d. As the load increases and reaches the occurrence of an impending brittle failure, an abrupt increase of the slope of the cumulative counts occurs. In this stage, RA values start to increase and AF values start to decrease. Some possible reasons for the change in RA and AF with the evolution of the damage have already been discussed in a study of AE signals from concrete in 4-point bending [45]. The AE waves travel through the material in different modes, depending on the source of the damage. For example, some types of damage cause a release of energy that is primarily converted into a longitudinal wave mode (P) of a large amplitude, which is parallel to the wave propagation. This kind of wave travels fast causing a short rise and a small

RA value. As the load increases, the wave travels in other wave modes such as shear waves (S), perpendicular to the wave propagation, or surface waves, mixed of P and S waves, due to scattering of damage in the specimen. These types of waves are slower than the longitudinal waves, which results in a longer rise time and larger RA value.

In the present work, there is also a change in the magnitude of both RA and AF that is correlated with the changes in the slope of the cumulative counts. It can be observed that at the failure of GFRP size 6 or before failure of GFRP size 4 in Fig. 8a, b, RA decreases and AF increases. This change could be related to the delaminating of the outside layer of the GFRP, which was observed with the naked eye. In contrast, CFRP size 2 shows a continuous increase in RA value as shown in Fig. 7a, which may be due to some elongation in the matrix that was observed in the longitudinal section sample. This elongation will be shown later in the SEM section. On the other hand, these changes in the RA and AF values were not observed in CFRP size 4 specimen, which were loaded up to 93% of the
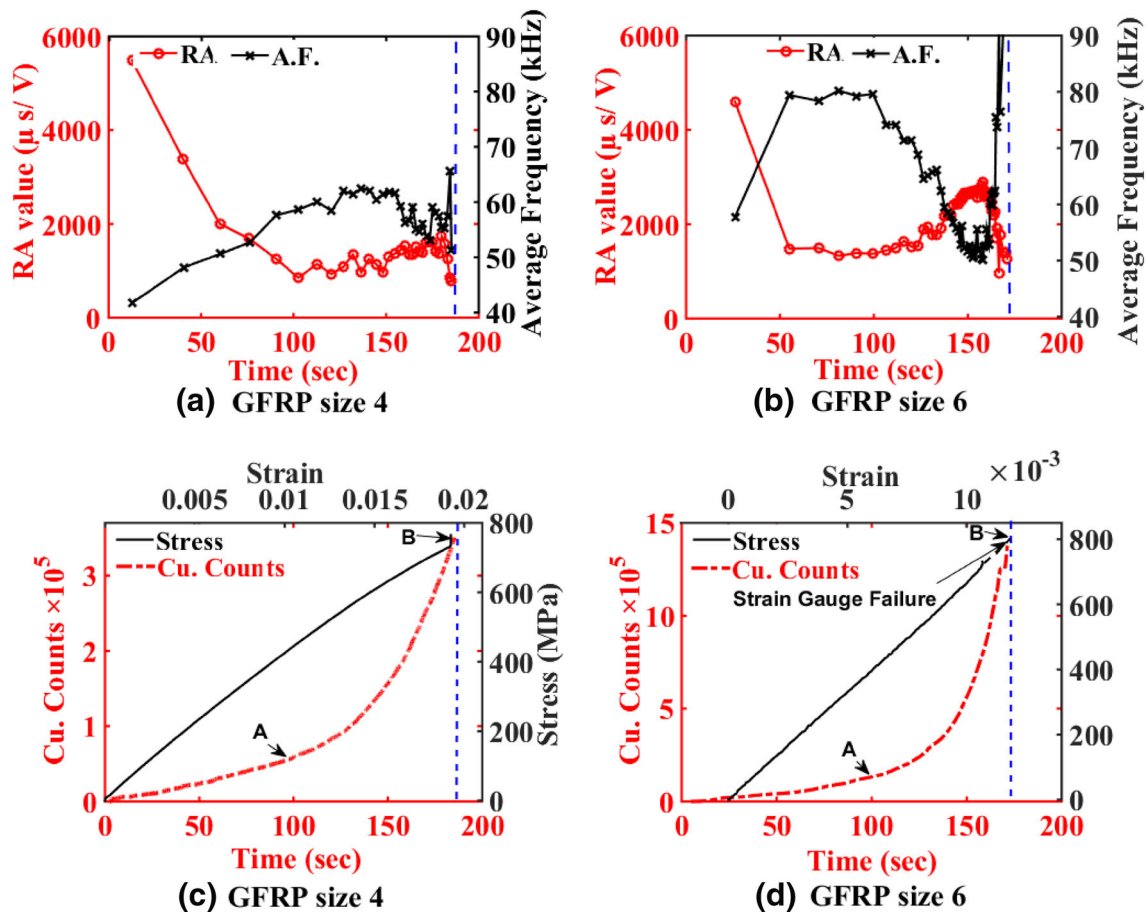
Fig. 8 Variation of AF and RA values. Cumulative counts vs. time with stress–strain superimposed. Dashed line represents time at which failure occurred for GFRP size 6. GFRP size 4 was loaded up to 95% of the predicted ultimate load

predicted ultimate load. A longitudinal section of the CFRP size 4 specimen after the load test did not show transverse cracks using SEM observation, which is consistent with the AE observations.

It should be pointed out that the changing of the slope of the cumulative counts as shown in Figs. 7c, d and 8c, d is not mimicked in the stress versus strain graph. A summary of these results is shown in Table 2 for both CFRP and GFRP specimens.

In conclusion, the slope of the cumulative counts increases with increasing load. However, the absolute number of events at failure varies considerably from specimen to specimen, and by itself is not reliable predictor of failure.

6.1.3 Amplitude–duration

The amplitude and duration of the AE events has been used to check the quality of the recorded data and to correlate with the type of damage mechanism [46]. Research on short glass fiber composites has been conducted for linking damage identification to the amplitude and duration

parameters [47]. The results showed that increases in the average magnitude of these parameters are an indication of damage evolution during loading [47].

In this study, the duration of each AE signal for one specimen was plotted in Fig. 9, as a function of amplitude for the three stages that were determined in Table 2. Based on the evaluation criteria in [48], events with high amplitude and long duration were attributed to fiber breakage. Low to medium amplitude events with low to medium duration were attributed to matrix cracking [48]. Similar results were also observed in studies on composite laminates [49] and GFRP bridge deck panels [50].

Figure 9 plots the duration of AE signal versus its amplitude. The results in Fig. 9 are clustered in a well-banded area, with very few outliers outside the banded area. Previous research correlated these outlier events as unwanted signals that could be either due to Electromagnetic interference, Mechanical rubbing (MR), or overlapping events (OE) [51]. The data presented in Fig. 9 indicate few of these unwanted events. Considering the scarcity of the unwanted events, the testing setup was satisfactory.

Table 2 AE Signal Parameters for CFRP and GFRP specimens

	Point on the cumulative counts curve	RA[a] value range[b] (μs/V)	AF[a] value range (kHz)	Strain[a] range (%)	Load[a] range (kN)	Percentage of the predicted ultimate load range (%)
CFRP size 2	A	952–1366	48–60	0.67–1.04	32–45	44–55
	B	810–1588	29–64	0.90–1.15	29–64	60–72
	C	1200–1560	26–60	1.10–2.10	55–75	75–96
	D	2589–8557	31–60	1.24–2.20	73–87	100
CFRP size 4	A	1389–2823	58–85	0.15–0.24	15–59	5–22
	B	1140–1756	68–100	0.55–0.93	126–188	47–70
	C	835–1077	81–83	1.33–1.51	250–290	93–100
GFRP size 4	A	465–1378	58–75	0.93–1.00	44–58	42–50
	B	741–1256	51–83	1.68–1.96	99–117	90–100
GFRP size 6	A	787–1890	70–80	0.54–0.85	96–142	40–62
	B	1047–2271	50–92	1.19–1.92	216–241	92–100

[a] RA, AF, Strain, and Load are the values at the change of the slope of the cumulative counts curve

[b] Range is the range of results when point (A, B, C, D) was reached for the FRP samples tested
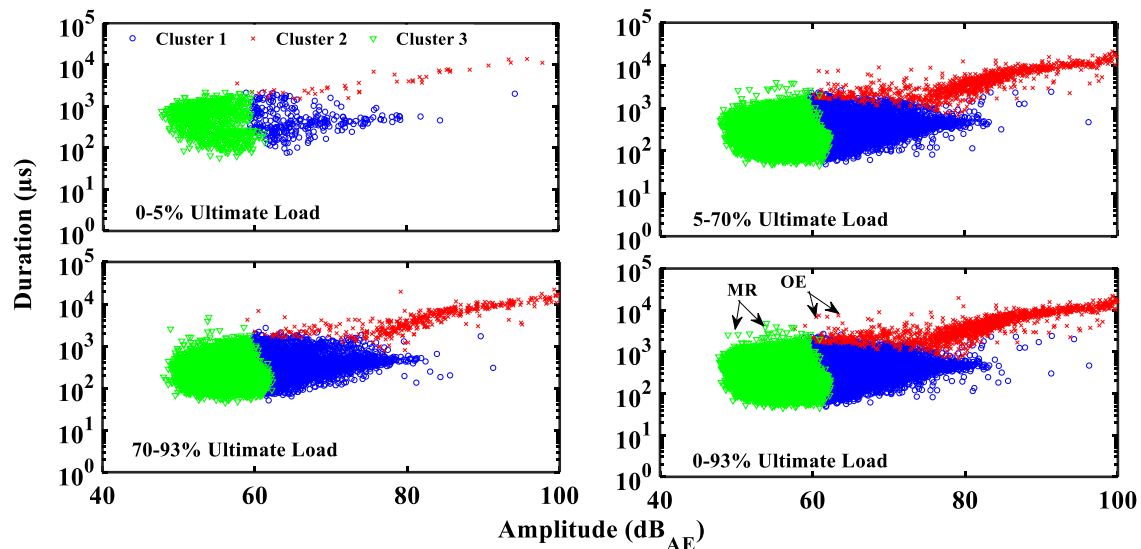

Fig. 9 Duration vs. Amplitude for three stages in CFRP size 4 specimen. Duration is the time of a signal from the first point exceeding the threshold level to the last one. *MR* mechanical rubbing, *OE* overlapping events, *cluster 1* deboning, *cluster 2* fiber breakage, *cluster 3* matrix cracking

Pattern recognition techniques have proven valuable for AE signals classification [52–54]. In the present work, a *k* means algorithm [55] was used to classify the AE signals. In this case, the *k* means algorithm used five parameters in time domain as the input data. The parameters used were peak amplitude, duration, counts, energy, and rise time as described in Fig. 1. The algorithm classifies the input data depending on a predefined number of clusters, which was set to three to match the expected types of damage. The types of damage will be discussed in the SEM section later in this paper. The principle of this method is to minimize the sum of the squared distance between the assigned cluster and its center. After that, the cluster vector and its centroid are iteratively actualized until the centroid is fixed. The classification was replicated five times each time with randomly assigned initial conditions.

Based on previous published articles [51] and the experimental data, most likely cluster 1 corresponds to debonding, cluster 2 corresponds to fiber breakage, and cluster 3 corresponds to matrix cracking. Also, the figure shows that these three clusters were observed in all three stages of the test. It should be noted that some signal misclassification could be due to the signal attenuation from the source to the sensor. Attenuation will result in

amplitude and duration reduction, so an event that is classified as matrix cracking or debonding could have originally been due to fiber breakage mode.

It can be concluded from Fig. 9 that the peak amplitude is correlated with the duration and that larger amplitude signals tend to also be of longer duration. This may in part be due to the duration from the first to the last threshold crossing being longer for higher-amplitude events, simply because higher-amplitude events will take more cycles to ring down. The number of AE signals within the various amplitude ranges was investigated in CFRP and GFRP specimens. The mean of AE features, such as duration and rise time, for each range was calculated for the three stages described in Table 2. The results showed that the CFRP signals have a mean duration and mean rise time that are less than GFRP signals at the start of the test, but they are larger as the load increases after about 40% of the predicted ultimate load.

6.2 AE signal Analysis in time–frequency domain

Time-varying signals were analyzed in terms of time–frequency domain using STFT to determine the frequency magnitudes that were predominant during the tension test. AE signals that were generated during the test are associated with the magnitude of the released strain energy. Accordingly, these AE signals have specific characteristics due to their amplitude, duration, and frequency content that could be related to a specific damage mechanism [56]. The nonstationary nature of the AE signal limits the choice of the time window length for STFT; therefore, for acceptable spectral resolution the length of window should be at least the same size as is the longest signal duration. In the current study, a signal was divided into sections of length of 128 samples with overlapping of 120 samples using Hamming windows, and the spectrum was evaluated at 129 frequencies according to [53]. This leads to a 20-µs time window length. In the time–frequency plot, energy in the signal is represented by calculating the squared coefficient of STFT matrix in MATLAB. STFT was performed on different AE signal amplitudes, and then energy distribution is calculated using the formula in Eq. 1, and plotted in Fig. 10 as a function of frequency content. In fact, the 80–200 kHz resonant sensor could limit the results of the frequency ranges. Most of the energy lies in the range of 125–180 kHz in CFRP with some small peaks between 80 and 125 kHz. While they are distributed in almost all frequency ranges for GFRP for 98 dB$_{AE}$ signal amplitude which indicates that several types of damage could be occurring simultaneously. For example, a fiber breakage is more likely to be accompanied with other kinds of damage such as fiber pull out or the movement of the fiber. For 85 dB$_{AE}$ signal amplitude, the peak frequency is about 136 kHz for CFRP, while the frequencies are distributed equally between 110 and 160 kHz for GFRP. For 75 dB$_{AE}$ signal amplitude, the energy lies in the frequency range of 150–180 kHz for CFRP and is distributed equally between 80 and 200 kHz in GFRP. A similar pattern can be seen in the 65 dB$_{AE}$ signal.

7 SEM observation

Typically, no damage is visible in the FRP bars to the naked eye until failure and, therefore, SEM analysis was used for microstructural examination. Transverse and longitudinal sections were cut from each bar before and after testing. Clean and flat sections were prepared using the following procedures: the samples were mounted into epoxy to prevent surface damage during the cutting process, and then a slow-speed diamond saw was used to cut them. After that, the sections were polished to remove marks generated during the cutting process, and to get a smooth surface for imaging. The polishing started with 40 and 30 µm silicon carbide sand paper, followed by 5 and 1 µm alumina slurry with a nylon cloth. The polished sections were cleaned using ultrasound bath with ethanol, and then coated with gold palladium.

Figure 11 shows the SEM images of both CFRP and GFRP rebar samples. The micrographs were acquired in the secondary and backscattered electron modes at an accelerating voltage of 15 kV and magnification range of 100x–600x. After loading CFRP size 2 to failure and GFRP size 4–95% of the predicted ultimate load, three types of damage were observed in the longitudinal sections: matrix cracking that developed longitudinally parallel to the fiber direction, debonding, and fiber fracture. On the other hand, no transverse matrix cracking was observed in the cross section sample; Only enlargement of the original voids was detected. In the CFRP size 2 sample, the longitudinal section showed misalignment of fibers, which indicated damage in the matrix. In general, modulus of elasticity of fibers is higher than the one for matrix; therefore, some fibers were fractured throughout the specimens with increasing load. Most of the fracture occurred due to splitting of the outside layer of the bars at failure as shown in Fig. 11h. It can be concluded from these observations that the damage tends to start near the voids. The void concentration was higher in the outside layer leading to the damage propagation in this layer at loads closer to failure.
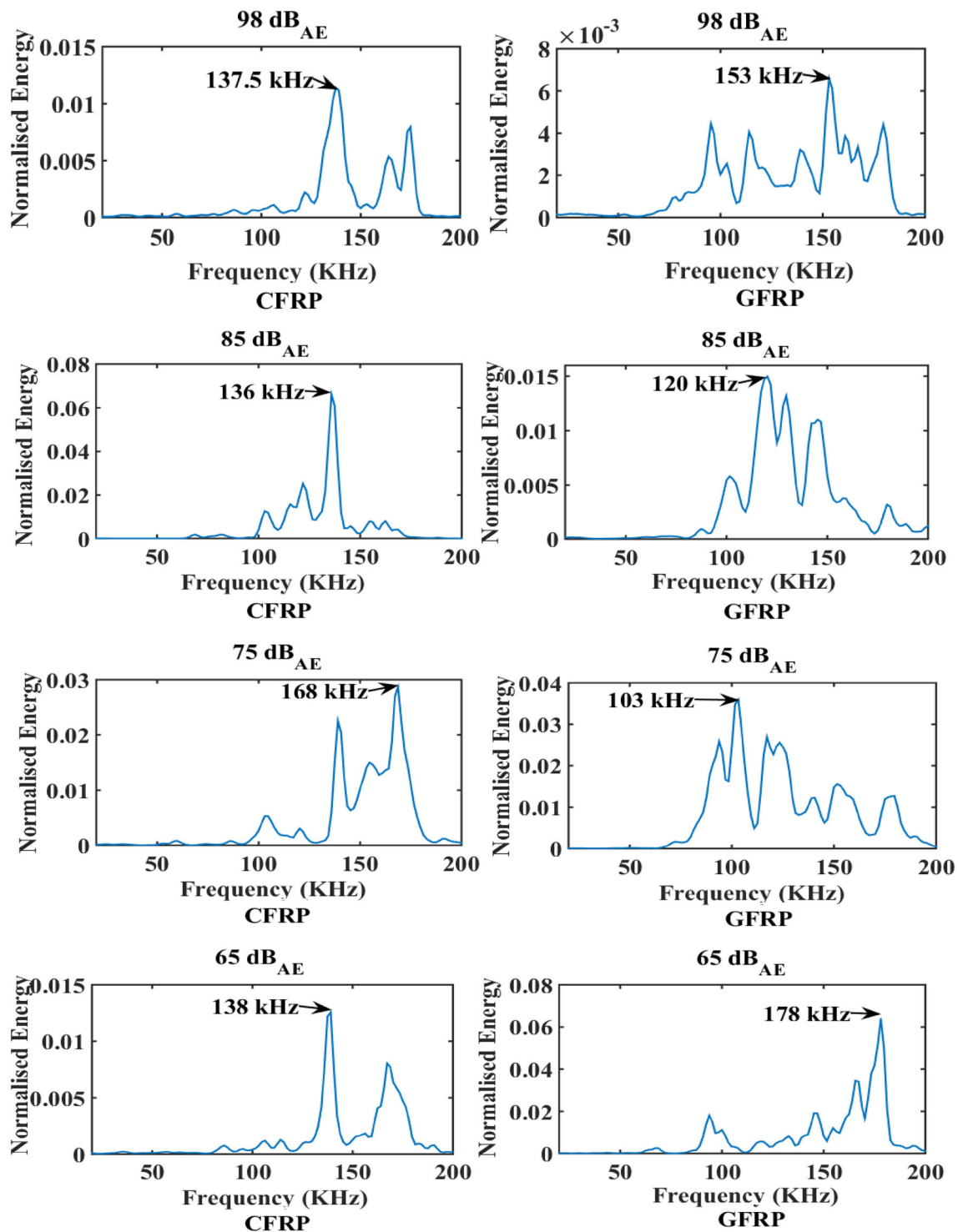
Fig. 10 Energy distribution versus frequency content for various signal amplitude for CFRP and GFRP bar specimens

8 Conclusions

In this work, the acoustic emission behavior of different diameters of CFRP and GFRP bar specimens under fracture stress in tensile loading was investigated. AE signals generated from damage were detected by piezoelectric transducers that were attached to the specimens' anchorage surface. The AE signals were analyzed using the RMS AE hit detection algorithm, and then parameters were extracted in time and time–frequency domain. The results of 20 FRP bar specimens showed that AE parameters changed as the
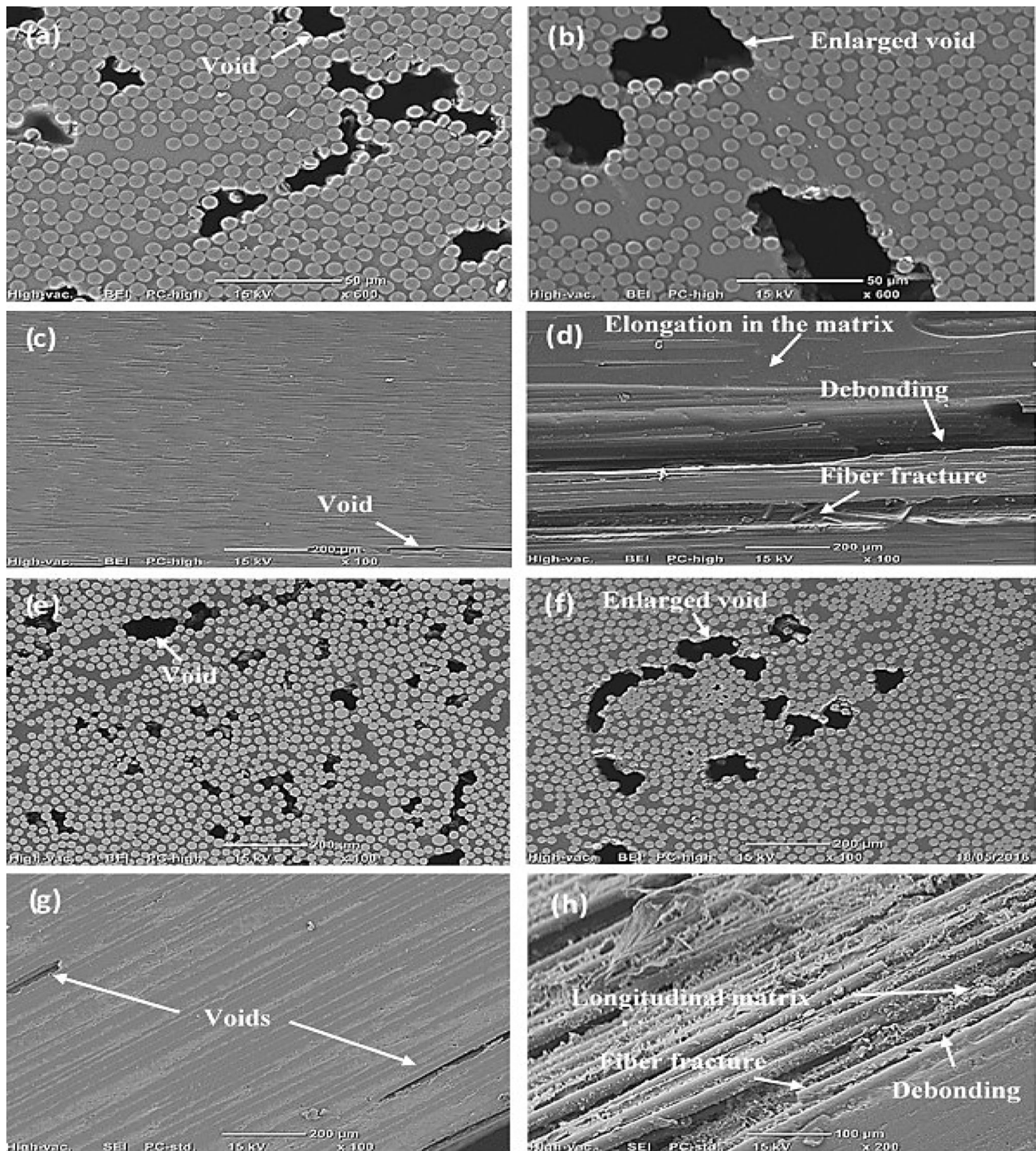
Fig. 11 SEM micrograph for untested and tested CFRP size 2 and GFRP size 4 bar specimens. **a** Cross section for untested CFRP size 2 specimen. **b** Cross section for tested CFRP size 2 specimen until failure; **c** longitudinal section for untested CFRP size 2 specimen; **d** longitudinal section for tested CFRP size 2 specimen until failure; **e** cross section for untested GFRP size 4 specimen; **f** cross section for tested GFRP size 4 specimen until failure; **g** longitudinal section for untested GFRP size 4 specimen; **h** longitudinal section for tested GFRP size 4 specimen until failure. The scale bar equals to: (50 μm for **a** and **b**; 200 μm for **c**–**f**, and g; 100 μm for **h**) images

quasi static load on the bar was increased. FRP is a linear elastic material and the stress–strain curves were linear until failure and did not show any indication of increasing damage.

In previous work, the observed changes in AE parameters, similar to those reported in this work, have been correlated with the occurrence of different damage mechanisms in FRP materials. With pultruded FRP bars, AE signals with high

amplitude and duration occur more frequently as the load approaches the ultimate load, while the low to medium amplitude signals appeared throughout the testing period. The RA and AF also showed some correlation with the increasing the slope of cumulative counts curve. In CFRP, the increasing of RA and decreasing of AF refer to the elongation in the matrix. In GFRP, the decreasing of RA and increasing of AF refer to the delaminating of the outside layer. Moreover, AE signals generated from CFRP bars have a shorter duration than GFRP bars. The mean values were equal to 16.16 ms during the last third of the test time for CFRP bars, and 20.24 ms for GFRP bar. CFRP bars have higher amplitude signals than GFRP. Specifically, the ratio of high to the sum of low and medium amplitude events is 4% for CFRP size 2, 6% for CFRP size 4, and 1% for both GFRP size 4 and 6. In addition, frequency peaks were obtained using STFT and energy distribution. Most AE signals have more than one frequency band, which indicates that different damage mechanisms occurred at the same time of the real-time testing. These peaks are limited to the sensitivity of the resonant transducer, R15I-AST of 80–200 kHz frequency range. Future study should be done using a broadband transducer.

SEM investigation revealed three types of damage in the longitudinal sections: matrix cracking that started from the voids and developed at the same direction of the fibers, debonding, and fiber fracture. On the other hand, the transverse sections did not show any transverse matrix cracking; just the enlargement of the voids which indicate that the matrix cracking occurred at regions between voids. In contrast, AE analysis revealed different number of events for different specimens of the same type of FRP bar, and that is due to different void volume fraction that was observed under SEM investigation. This work contributes to better understanding the behavior of these bars and future research aimed at finding a method of determining the in service stress and damage level.

The experimental results from the AE monitoring system could be used to identify different stages of internal damage of the specimens related to micro-crack propagation and the failure of FRP bars. The results also confirmed that the slope of the cumulative counts increases with increasing load. However, the large variation of the absolute number of events at failure makes it a poor metric to predict when FRP bars will fail. Furthermore, the time–frequency characteristics determined from different signal amplitudes are different and may be performed for different damage identification. Further research is necessary to classify damage modes throughout the test.

References

1. El Batanouny M, Larosche A, Mazzoleni P, Ziehl P, Matta F, Zappa E (2014) Identification of cracking mechanisms in scaled FRP reinforced concrete beams using acoustic emission. Exp Mech 54(1):69–82
2. Mirmiran A, Philip S (2000) Comparison of acoustic emission activity in steel-reinforced and FRP-reinforced concrete beams. Constr Build Mater 14(6):299–310
3. Yun H-D, Choi W-C, Seo S-Y (2010) Acoustic emission activities and damage evaluation of reinforced concretebeams strengthened with CFRP sheets. NDT and E Int 43(7):615–628
4. J.P. Busel. (2016). Introduction to fiber reinforced polymer (FRP) composites in infrastructure, American Composites Manufacturers Association(ACMA)
5. Gross CU, Ohtsu M (eds) (2008) Acoustic emission testing: basics for research—applications in civil engineering. Springer, Berlin Heidelberg. https://doi.org/10.1007/978-3-540-69972-9
6. ASTM E1316 (2006) Standard terminology for non-destructive examinations. American Standard for Testing and Materials, pp. 1–33
7. Vidya Sagar R, Raghu Prasad BK (2013) Laboratory investigations on cracking in reinforced concrete beams using on-line acoustic emission monitoring technique. J Civ Struct Health Monit 3:169–186. https://doi.org/10.1007/s13349-013-0036-5
8. Abouhussien AA, Hassan AAA (2015) Evaluation of damage progression in concrete structures due to reinforcing steel corrosion using acoustic emission monitoring. J Civ Struct Health Monit 5:751–765. https://doi.org/10.1007/s13349-015-0144-5
9. Ziehl PH (2000) Development of a damage based design criterion for fiber reinforced vessels, Dissertation, University of Texas at Austin
10. Barre S, Benzaggagh ML (1992) On the use of acoustic emission to investigate damage mechanisms in glass fibre-reinforced polypropylene. Compos Sci Technol 52(3):369–376
11. Rizzo P, di Scalea FL (2001) Acoustic emission monitoring of carbon fiber-reinforced-polymer bridge stay cables in large-scale testing. Exp Mech 41(3):282–290
12. Ely TM, Hill EVK (1995) Longitudinal splitting and fiber breakage characterization in graphite epoxy using acoustic emission data. Mater Eval 53(2):288–294
13. Komai K, Minoshima K, Shibutani T (1991) Investigation of the fracture mechanism of carbon/epoxy composites by AE signal analysis. JSME Int J 34(3):381–388
14. Suziki M, Nakanishi H, Iwamoto M, Jinen E (1998) Application of static fracture mechanisms to fatigue fracture behaviour of class A-SMC composite. In: Proc. 4th Japan-US Conference on Composite Materials, pp. 297–306
15. Chen HL, Sami Z, GangaRao H. V (1993) Identifying damages in stressed aramid FRP bars using acoustic emission. Dynamic Characterization of Advanced Materials, ASME NCA-Vol. 16/AMD-Vol. 172, ASME, New York, 171–178
16. Liang Y, Sun C, Ansari F (2004) Acoustic emission characterization of damage in hybrid fiber reinforced polymer rods. J Compos Constr 8(1):70–78
17. Liang Y, Sun C, Ansari F (2011) Damage assessment and ductility evaluation of post tensioned beams with hybrid FRP tendons. J Compos Constr 15(3):274–283
18. Stevenson S, Mohammad K, Svecova D, Thomson D (2014) Study of acoustic emission signals for detection of impending

failure of FRP bars. In: Composites in Civil Engineering Conference, 2014

19. De Groot PJ, Wijnen PAM, Janseen RBF (1995) Real-time frequency determination of acoustic emission for different fracture mechanisms in carbon/epoxy composites. Compos Sci Technol 55(4):405–412

20. Gutkin R, Green CJ, Vangrattanachai S, Pinho ST, Robinson P, Curtis PT (2011) On acoustic emission for failure investigation in CFRP: pattern recognition and peak frequency analyses. Mech Syst Signal Process 25(4):1393–1407

21. Hamstad MA, O'Gallagher A, Gary J (2002) A wavelet transform applied to acoustic emission signals: part 1: source identification. J Acoust Emiss 20:39–61

22. Kaphle M, Tan ACC, Thamberatnam DP, Chan THT (2011) Study of acoustic emission data analysis tools for structural health monitoring applications. J Acoust Emiss 29:243–250

23. Kaphle M, Tan ACC, Thamberatnam DP, Chan THT (2012) Effective discrimination of acoustic emission source signals for structural health monitoring. Advances in Structural Engineering 15(5):707–716

24. Siegmann A, Kander RG (1992) In-situ acoustic emission monitoring during electron microscopy of a model composite system. Polym Compos 13(2):108–120

25. Ramirez-Jimenez CR, Papadakis N, Reynolds N et al (2004) Identification of failure modes in glass/polypropylene composites by means of the primary frequency content of the acoustic emission event. Compos Sci Technol 64:1819–1827. https://doi.org/10.1016/j.compscitech.2004.01.0081

26. ASTM F1430 (2005) Standard Test Method for Acoustic Emission Testing of Insulated and Non Insulated Aerial Personnel Devices with Supplemental Load Handling Attachments1. An American National Standard, pp 1–10

27. ASM International Handbook Committee (1989) ASM handbook, volume 17—nondestructive evaluation and quality control. ASM International, Metals Park, Ohio, pp 278–294

28. CSA standard (2012) Design and construction of building structures with fibre-reinforced polymers. CSA S806-12, Canadian Standards Association, Mississauga, pp 90–92

29. Czichos H (ed) (2013) Handbook of technical diagnostics, fundamentals and application to structures and systems. Springer, Berlin Heidelberg, pp 137–160

30. Maillet E, Godin N, R'Mili M, Reynaud P, Fantozzi G, Lamon J (2014) Real-time evaluation of energy attenuation: a novel approach to acoustic emission analysis for damage monitoring of ceramic matrix composites. J Eur Ceram Soc 34(7):1673–1679

31. Chapra SC, Canale RP (2012) Numerical methods for engineers. McGraw-Hill, New York

32. Shateri M, Ghaib M, Svecova D, Thomson DJ (2017) On acoustic emission for failure prediction in fiber reinforced polymer rods using pattern recognition analysis. Smart Mater Struct 26(6):065023

33. Barre S, Benzaggagh ML (1994) On the use of acoustic emission to investigate damage mechanisms in glass fibre-reinforced polypropylene. Compos Sci Technol 52(3):369–376

34. Bhat MR, Majeed MA, Murthy CRL (1994) Characterization of fatigue damage in unidirectional GFRP composites through acoustic emission signal analysis. NDT E Int 27(1):27–32

35. Drummond G, Watson JF, Acarnleyb PP (2007) Acoustic emission from wire ropes during proof load and fatigue testing. NDT E Int 40(1):94–101

36. Bai W, Chai M, Li L, Li Y, Duan Q (2015) Acoustic emission from elevator wire ropes during tensile testing, In: advances in acoustic emission technology: Proceedings of the World Conference on Acoustic Emission-2013. Springer Proceedings in Physics 158, Shen G, Wu Z, Zhang J (eds.), 138, New York, pp. 217–224

37. Ohno K, Ohtsu M (2010) Crack classification in concrete based on acoustic emission. Constr Build Mater 24(12):2339–2346

38. Aggelis DG (2011) Classification of cracking mode in concrete by acoustic emission parameters. Mech Res Commun 38(3):153–157

39. JCMS-IIIB5706 (2003) Japan construction material standards monitoring method for active cracks inconcrete by acoustic emission. The Federation of Construction Material Industries, Japan

40. Suzuki T, Ohtsu M (2005) Practical application of water-leaked pipeline by AE parameter analysis In: Proc. 3rd US-Japan Sym, Advancing Application and Capabilities in NDEASTM, Hawaii, pp 202–208

41. Soulioti D, Barkoula NM, Paipetis A, Matikas TE, Shiotani T, Aggelis DG (2009) Acoustic emission behavior of steel fibre reinforced concrete under bending. Constr Build Mater 23(12):3532–3536

42. Anastassopoulos AA, Philippidis TP (2010) Clustering methodology for evaluation of acoustic emission from composites. J Acoust Emiss 13(1/2):11–22

43. Aggelis DG, Barkoula NM, Matikas TE, Paipetis AS (2010) Acoustic emission monitoring of degradation of cross ply laminates. J Acoust Soc Am 127(6):246–251 (EL)

44. Ramirez-Jimenez CR, Papadakis N, Reynolds N, Gan TH, Purnell P, Pharaoh M (2004) Identification of failure modes in glass/polypropylene composites by means of the primary frequency content of the acoustic emission event. Compos Sci Technol 64(12):1819–1827

45. Aggelis DG, Soulioti DV, Sapouridis N, Barkoula NM, Paipetis AS, Matikas TE (2011) Acoustic emission characterization of the fracture process in fibre reinforced concrete. Constr Build Mater 25(11):4126–4131

46. CARP (1999) Recommended Practice for Acoustic Emission Evaluation of Fiber Reinforced Plastic (FRP) Tanks and Pressure Vessels. The Committee on Acoustic Emission for Reinforced Plastics (CARP), A Division of the Technical Council of the American Society for Nondestructive Testing, Inc., Columbus, Ohio, Draft I

47. Nguyen BN, Tucker BJ, Khaleel MA (2005) A Mechanistic approach to matrix cracking coupled with fiber–matrix debonding in short-fiber composites. J Eng Mater Technol 127(3):337–350

48. Committee on Acoustic Emission from Reinforced Plastics _CARP (1987) Recommended practice for acoustic emission testing of fiberglass reinforced plastic resin _RP_ tanks/vessels. Composites Institute, Society of the Plastics Industry, New York

49. Gudmundson P, Johnson M (2000) Transient recording and analysis of acoustic emission events resulting from damage evolution in composite laminates. In: Proc., 15th World Conf. on Non-Destructive Testing, Rome, International Committee for Nondestructive Testing

50. Gostautas RS, Ramirez G, Peterman RJ, Meggers D (2005) Acoustic emission monitoring and analysis of glass fiber-reinforced composites bridge decks. J Bridge Eng 10(6):713–721

51. Fowler T, Blessing J, Conlisk P (1989) New directions in testing. In: 3rd international symposium on AE from composite materials," NDT & E International, Paris, France, pp 16–27

52. Ono K, Huang Q (1994) Pattern recognition analysis of acoustic emission signals. Progress in acoustic emission VII. In: Proceedings of the 12th International Acoustic Emission Symposium, Sapporo (Japan). Edited by T. Kishi, Y. Mori and M. Enoki. The Japanese Society for NDI, pp 69–78

53. Mathworks, "MATLAB Users Guide," Natick, MA 2009. http://www.mathworks.com

54. Godin N, Huguet S, Gaertner R (2005) Integration of the Kohonen's self-organising map and k means algorithm for the

segmentation of the AE data collected during tensile tests on cross-ply composites. NDT E Int 38(4):299–309

55. Arthur D, Vassilvitskii S (2007) K-means ++: the advantages of careful seeding. In: SODA '07: Proceedings of the Eighteenth Annual ACM-SIAM Symposium on Discrete Algorithms, pp 1027–1035

56. Yang BL, Zhuang XM, Zhang TH, Yan X (2009) Damage mode identification for the clustering analysis of AE signals in thermoplastic composites. J Nondestr Eval 28(3):163–168